ChemPhotoChem

Research Article
doi.org/10.1002/cptc.202300155

Chemistry Europe
European Chemical Societies Publishing

www.chemphotochem.org

Au-Catalyzed Energy Release in a Molecular Solar Thermal (MOST) System: A Combined Liquid-Phase and Surface Science Study

Roman Eschenbacher[+],[a] Felix Hemauer[+],[b] Evanie Franz,[a] Andreas Leng,[c] Valentin Schwaab,[b] Natalie J. Waleska-Wellnhofer,[b] Eva Marie Freiberger,[b] Lukas Fromm,[d] Tao Xu,[a] Andreas Görling,[d] Andreas Hirsch,[c] Hans-Peter Steinrück,[b] Christian Papp,[b, e] Olaf Brummel,*[a] and Jörg Libuda[a]

Molecular solar thermal systems (MOSTs) are molecular systems based on couples of photoisomers (photoswitches), which combine solar energy conversion, storage, and release. In this work, we address the catalytically triggered energy release in the promising MOST couple phenylethylesternorbornadiene/quadricyclane (PENBD/PEQC) on a Au(111) surface in a combined liquid-phase and surface science study. We investigated the system by photoelectrochemical infrared reflection absorption spectroscopy (PEC-IRRAS) in the liquid phase, conventional IRRAS and synchrotron radiation photoelectron spectroscopy (SRPES) in ultra-high vacuum (UHV). Au(111) is highly active towards catalytically triggered energy release. In the liquid phase, we did not observe any decomposition of the photoswitch, no deactivation of the catalyst within 100 conversion cycles and we could tune the energy release rate of the heterogeneously catalyzed process by applying an external potential. In UHV, submonolayers of PEQC on Au(111) are back-converted to PENBD instantaneously, even at 110 K. Multilayers of PEQC are stable up to ~220 K. Above this temperature, the intrinsic mobility of the film is high enough that PEQC molecules come into direct contact with the Au(111) surface, which catalyzes the back-conversion. We suggest that this process occurs via a singlet–triplet mechanism induced by electronic coupling between the PEQC molecules and the Au(111) surface.

Introduction

Besides the established technologies to harvest and store solar energy, such as photovoltaics, batteries, or power-to-X technologies, there are also very simple molecular approaches. One example are molecular solar thermal systems (MOSTs), which combine solar energy conversion, storage, and release using switchable photoisomers (photoswitches).[1–5] In this approach, an energy-lean isomer is converted photochemically in a one-photon one-molecule process into its metastable energy-rich isomer. In this way, the solar energy is stored chemically. The stored energy can be released as thermal energy when an appropriate trigger is applied. Different classes of photoswitches may serve as MOSTs, e.g., the E/Z-azobenzene couple (E/Z-AZO),[6–11] the dihydroazulene/vinylheptafulvene couple (DHA/VHF),[12–14] and the azaborine/BN-dewar couple (AB/ABD).[15] One of the most studied MOST systems, is the norbornadiene/quadricyclane pair (NBD/QC).[4,16–20] The pristine NBD/QC couple reaches an energy density of 100 kJ·mol^{-1} (1 MJ·kg^{-1}),[4] which is similar to state-of-the-art Li-ion batteries. However, NBD absorbs light only in a very small spectral region (below 300 nm)[4] of the solar spectrum (100 nm to 1 mm),[21] which limits its applicability. To overcome this issue, researchers developed a variety of different NBD/QC derivatives with additional push-pull ligands, which shift the absorption maximum to the red and enable a better match with the solar spectrum.[22–25]

[a] R. Eschenbacher,[+] E. Franz, Dr. T. Xu, Dr. O. Brummel, Prof. Dr. J. Libuda
Interface Research and Catalysis
Erlangen Center for Interface Research and Catalysis
Friedrich-Alexander-Universität Erlangen-Nürnberg
Egerlandstraße 3, 91058 Erlangen (Germany)
E-mail: olaf.brummel@fau.de

[b] F. Hemauer,[+] V. Schwaab, N. J. Waleska-Wellnhofer, E. M. Freiberger, Prof. Dr. H.-P. Steinrück, Prof. Dr. C. Papp
Lehrstuhl für Physikalische Chemie II
Friedrich-Alexander-Universität Erlangen-Nürnberg
Egerlandstraße 3, 91058 Erlangen (Germany)

[c] A. Leng, Prof. Dr. A. Hirsch
Lehrstuhl für Organische Chemie II
Friedrich-Alexander-Universität Erlangen-Nürnberg
Nikolaus-Fiebiger-Straße 10, 91058 Erlangen (Germany)

[d] Dr. L. Fromm, Prof. Dr. A. Görling
Lehrstuhl für Theoretische Chemie
Friedrich-Alexander-Universität Erlangen-Nürnberg
Egerlandstraße 3, 91058 Erlangen (Germany)

[e] Prof. Dr. C. Papp
Angewandte Physikalische Chemie
Freie Universität Berlin
Arnimallee 22, 14195 Berlin (Germany)

[+] Theses authors contributed equally to this work.

Supporting information for this article is available on the WWW under https://doi.org/10.1002/cptc.202300155

One aspect, which is equally important, but received less attention so far, is the controlled energy release in MOST systems.[4] The most promising approaches to trigger the energy release are by a heterogeneous catalyst[23,26–29] or by a electrochemical process.[6,30–34] In a recent study, we combined the advantages of both approaches. For a specific NBD/QC couple, we demonstrated that the catalytic activity of Au(111) is very high (exceeding the activity of Pt(111) by a factor of 200 in the liquid phase). In addition, we showed that the catalytic activity can be tuned by an externally applied potential. Here, it is important to note that the reaction was always triggered by a catalytic process and not by an electrochemical reaction.[35] In stability tests, the system remained operational over 1000 conversion cycles without any side product formation detected. Moreover, the observed loss in catalytic activity was less than 0.1% per cycle demonstrating the outstanding catalytic properties of Au(111).[35] For this study, the phenylethylester-substituted molecule pair PENBD/PEQC was chosen due to its promising properties concerning applicability as MOST system. The characterization after synthesis revealed not only a distinct redshift of the absorption onset of the NBD derivative to 359 nm with a reasonable quantum yield ($\Phi_{isom} = 71\%$ without photosensitizer)[23] but also a very pronounced thermal stability of the PEQC isomer (half-life of 450 days at room temperature). In addition, these isomers provide a high energy storage capacity of 367.5 kJ kg^{-1}.[36] Moreover, the surface chemistry of both PENBD and PEQC has already been investigated by synchrotron radiation-based XPS on different catalyst surfaces, namely Pt(111) and Ni(111).[37] In addition, the electrocatalytically triggered energy release of PEQC on HOPG was observed in PEC-IRRAS experiments before.[34] Yet, the catalytic activity and/or selectivity of the energy-releasing cycloreversion reaction was not ideal on the catalyst materials considered previously. Therefore, we investigate the PENBD/PEQC system on gold surfaces in the present study.[35,38] We apply a multimethod approach combining surface science techniques (IRRAS, SRPES) for a mechanistic understanding and liquid-phase experiments (PEC-IRRAS) to assess the performance and cyclability under realistic conditions. To gain a deeper mechanistic understanding of the catalytic processes, surface science studies in ultra-high vacuum (UHV) are required.[39] In the field of MOSTs, surface science studies demonstrated that the back-conversion reaction strongly depends on the catalyst surface. Moreover, these studies provided a detailed picture of the adsorption behavior, rearrangement steps, the stability limits, and decomposition pathways.[37,38,40–43] On Ni(111), pristine QC is stable in the submonolayer up to temperatures of ~175 K,[40] functionalized QC was found to be stable even up to 260 K.[42] In contrast, Pt(111) and Au(111) are much more reactive.[11,35,37,43] In direct contact with these surfaces, submonolayers of QC derivatives convert back even at ~100 K.[38] QC derivatives can only be stabilized in form of frozen multilayer films. It was proposed that the energy release on Au(111) is triggered by electronic coupling via a singlet-triplet mechanism. The gold substrate mediates an intersystem crossing between the singlets (S_0) and triplets (T_1) in the relaxation process resulting into minimized activation barriers; the mixing of quantum states of gold and molecular states enhances the isomerization rate drastically and reduces the direct chemical involvement of the surface.[29] For a NBD derivative with a TOTA anchoring platform on Au(111), we already suggested that the energy release occurs only if there is a direct electronic coupling to the gold.[38]

To finally prove the role of the electronic coupling in a liquid system, it is necessary to study the same NBD derivative in both environments, i.e., in the liquid phase under electrochemical control and in UHV. Herein, we present the results of such work.

Experimental

Synthesis

Phenylethylesternorbornadiene (PENBD): Freshly cracked cyclopentadiene (63.8 mmol, 4.22 g, 2 eq.) and ethyl-3-phenylpropiolate (31.9 mmol, 5.55 g, 1 eq.) were degassed with argon and heated to 180 °C overnight in a pressure vial. Afterwards, the mixture was purified via fractionated vacuum distillation using a Vigreux column (bp = 123 °C at 4.6×10^{-2} mbar) yielding the desired product as colorless oil, which solidified while storing in the freezer (−20 °C).

Yield: 4.59 g, 19.1 mmol, 60%.

Phenylethylesterquadricyclane (PEQC): For preparative photoisomerization, PENBD (300 mg, 1.25 mmol) was dissolved in $CDCl_3$ and irradiated in a quartz glass cuvette overnight, using a UV-LED (Seoul Viosys, CUD1AF4D, 310 nm, 30 mW). Subsequently, the crude product was purified via flash chromatography (hexane : EtOAc, 9.5 : 0.5) to obtain the title compound (294 mg, 1.23 mmol, 98%).

The UV/Vis spectra of both molecules were recorded on a J-815 CD spectropolarimeter from JASCO at 21 °C in acetonitrile (HPLC grade) and are provided in Figure 1. For further details on the syntheses we refer to literature.[23]

Liquid-phase experiments

Cleaning of the equipment: All PTFE and glassware was stored in a solution of NOCHROMIX® (Sigma Aldrich) and concentrated sulfuric acid (Merck, Emsure, 98%) overnight. Prior to the measurement, the equipment was rinsed 5 times with ultra-pure water (MilliQ Synergy UV, 18.2 MΩ cm at 298 K, TOC < 5 ppb) and boiled 3 times in Milli-Q water for at least 25 min. Finally, the equipment was dried in an evacuated desiccator overnight.

Photoelectrochemical infrared reflection absorption spectroscopy (PEC-IRRAS): All PEC-IRRA spectra were recorded using a vacuum-based Fourier-transform infrared (FT-IR) spectrometer (Bruker, Vertex 80v) with evacuated optics and a liquid nitrogen-cooled mercury cadmium telluride (MCT) detector. We used a scanner velocity of 240 kHz and a resolution of 8 cm^{-1} leading to an acquisition time of 0.5 s per spectrum. The setup was equipped with a UV-LED (Seoul Viosys, CUD1AF4D, 310 nm, 30 mW) underneath a CaF_2 hemisphere (Korth, d = 25 mm), which served as IR and UV-transparent window. The detector was protected by a KRS-5 filter. For details on the PEC-IRRAS setup we refer to our previous work.[44]

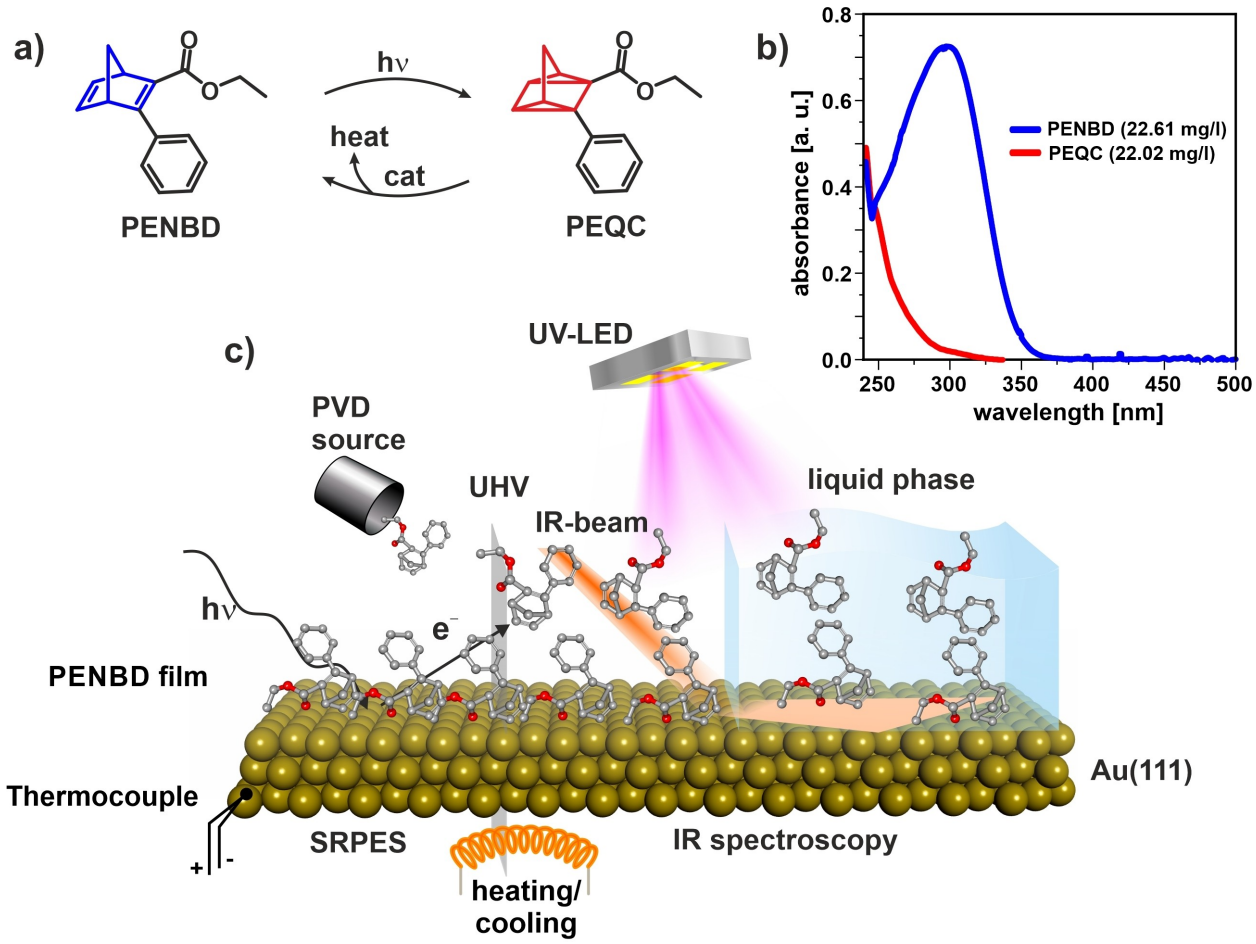

Figure 1. Schematic representation of the investigated system: a) Reaction scheme of the photochemical conversion and catalytically triggered back-conversion of PENBD/QC using Au(111) as catalyst; b) UV/Vis spectra of comparable concentrations of PENBD and PEQC; c) Overview of the different methods used in this study: SRPES (synchrotron radiation photoelectron spectroscopy), IR spectroscopy (infrared spectroscopy), PVD (physical vapor deposition) source, and UHV (ultra-high vacuum).

We cleaned the Au(111) single crystal (MaTeck, 99.999%, d = 10 mm, roughness < 10 nm, accuracy < 0.1°) in a freshly prepared piranha acid solution (H_2SO_4(conc.) : H_2O_2(30%), 2:1). Afterwards, we rinsed the crystal thoroughly with ultrapure water (MilliQ synergy UV, 18.2 MΩ cm at 25 °C, < 5 ppb TOC) and annealed the crystal in the flame of a Bunsen burner at orange glow for 3 min.[45] We measured PEC-IRRA spectra in reflectance mode using a thin-layer configuration. In all experiments, we used a solution of 10 mM PENBD with 0.1 M tetrabutylammoniumperchlorate (TBAP) (Sigma Aldrich, 99.0%) as supporting electrolyte in acetonitrile (MeCN) (Sigma-Aldrich, 99.999%). Potential control was provided by a commercial potentiostat (Gamry, Reference [600]) using a three-electrode configuration with a graphite rod as counter electrode and an Ag/Ag^+ electrode (0.01 M $AgNO_3$ with 0.1 M TBAP in MeCN) as reference electrode (RE). The calibration of the RE was performed in an external cell versus the cyclic voltammogram of ferrocene (Alfa Aesar, 99.5%). Note that in this work all potentials are referred to the redox potential of the ferrocene couple (V_{fc}).

Surface science experiments

IRRAS experiment: The sample cleaning and all IRRAS experiments were performed in an UHV setup with two sub-chambers and a base pressure of 1.0×10^{-10} mbar. The first sub-chamber is mainly used for sample preparation and consists of an ion gun (Specs IQE 11/35), electron beam evaporators (Focus EFM3), a LEED optics (Specs ErLEED 150), a quartz crystal microbalance (QCM, Inficon SQM-160), a gas dosing system, and a quadrupole mass spectrometer (QMS, Blazers Quadstar 422). The second measuring sub-chamber is equipped with multiple home-built Knudsen-cells, a QMS (Hiden Analytical Hal 3F), and a programmable effusive beam. IR spectra were measured with a vacuum Fourier-transform infrared (FTIR) spectrometer (Bruker VERTEX 80v) together with a liquid nitrogen-cooled mercury cadmium telluride (MCT) detector.

Sample preparation: The Au(111) single crystal (MaTeck) was cleaned with Ar^+ sputtering (Ar, Linde, > 99.9999%; 1.2 keV, 8×10^{-5} mbar, 60 min) and annealing (823 K in UHV; 10 min). LEED was used in order to check the structure of the sample.

PVD of PENBD: PENBD was evaporated from a glass reservoir. Prior deposition, the reservoir was evacuated via a rough pump. This reservoir is separated via a Swagelok valve from a home-built Knudsen cell, which is pumped by a separate high vacuum line. We monitored the uptake via IR spectra (rate of 1 min·spectrum^{-1}, spectral resolution of 4 cm^{-1}). Each spectrum was referenced to the clean surface recorded before the deposition. The growth rate was adjusted via the pressure in the chamber (~4.5×10^{-8} mbar).

Temperature programmed-IRRAS (TP-IRRAS or TP-IRAS): We carried out the TP-IRRAS experiment by heating the sample with a

linear heating ramp (2 K·min^{-1}) while recording IRRA spectra (1 min·spectrum^{-1}) simultaneously. The dampening of IR signals at higher temperatures was adjusted using a procedure by T. Xu et al..[46] Absolute spectra are obtained by using the last IRRA spectrum (measuring time of 10 minutes) at the end of the heating ramp of 700 K as a reference. The relative TP-IRRAS plot ($n = n_i/n_{i-1}$) was obtained by dividing each spectrum (n_i) by the previous spectrum (n_{i-1}).

Photochemical conversion in UHV: All photochemical experiments were performed in UHV using a home-built UV-source.[47] We used a high-power LED (Seoul Viosys, CUD1AF4D) with a peak wavelength of 310 nm and a typical forward voltage of 5.5 V. Power was supplied externally (PEAKTECH 6210) and we triggered the LED by a TTL signal from the spectrometer (Bruker OPUS 7.2).

Synchrotron radiation photoelectron spectroscopy (SRPES): The synchrotron radiation-based X-ray photoelectron spectroscopy experiments were conducted at beamline U49/2-PGM 1 of BESSY II (Helmholtz-Zentrum Berlin)[48] during multi-bunch top-up mode. All data were measured with a transportable ultra-high vacuum (UHV) apparatus, which is discussed in detail elsewhere.[49] The preparation of the sample was done in a dedicated chamber with typical surface science tools, such as a sputter gun, LEED optics, an electron beam evaporator, and a quartz crystal microbalance. The analysis chamber, separated by a gate valve, houses a quadrupole mass spectrometer, a hemispherical electron analyzer, and a directly attached evaporator for organic substances. XP spectra were recorded in normal emission (0°), and the angle of the incident light was 50°. The excitation energy of the photons was set to 380 and 650 eV, for probing the C 1s and O 1s regions, respectively, yielding resolutions of 150 meV (C 1s) and 250 meV (O 1s). All spectra were referenced to the Fermi level. For quantification, a linear background was subtracted and the signals were fitted with peaks consisting of a convolution of Gaussian and Doniach-Šunjić functions.[50] Coverages were calibrated by comparison with a saturated CO *c*(4 x 2) superstructure on Pt(111),[51] which equals $\theta_c = 0.5$ ML (that is, one carbon atom per every second surface atom).

As substrate for the SRPES measurements, we used a thin Au film deposited on a Pt(111) crystal; specifically, we evaporated a layer of 30 Å gold and annealed subsequently at 770 K for 10 min.[52–54] Gold deposition was calibrated with the built-in QCM. The Pt(111) crystal was cleaned by ion bombardment (Ar^+, E = 1.0 keV, I_s~8 μA) and annealed to 1200 K. Carbon contaminations were removed by exposure to oxygen at 850 K. The organic substances were purified with freeze-pump-thaw cycles and exposed to the surface at 110 K by their vapor pressure; the exposure is given in Langmuir (1 L = 10^{-6} Torr·s). Temperature-programmed experiments[55,56] up to 550 K were performed with a heating rate of 0.5 K·s^{-1}, utilizing a bifilar coiled filament behind the crystal. The sample was moved to a different position for every new spectrum to avoid beam damage effects by the intense X-ray radiation.

Results and Discussion

In Figure 1a, we depict the investigated MOST system phenylethylesternorbornadiene (PENBD) and its metastable QC derivative (PEQC). Upon irradiation, PENBD converted to the strained PEQC, thus storing part of the energy of the photon. We triggered the thermal energy release using Au(111) as heterogeneous catalyst. The experimental methods used in this study are illustrated in Figure 1b. We investigated the reaction kinetics, the reversibility, and the potential dependence of the energy-release reaction in the liquid phase by PEC-IRRAS. To obtain additional insights into the mechanism of back-conversion and desorption, we studied the behavior of submonolayers and multilayers of PENBD and PEQC by TP-SRPES and TP-IRRAS in UHV.

In Figure 2a and b, we show the IR spectra of PENBD and PEQC from gas-phase DFT calculations (top),[34] measurements in transmission mode at ambient pressure (middle)[34] and the multilayer IRRA spectra in UHV (bottom). We summarize the assignment of the IR bands in Table 1 and Table 2. We

Table 1. IR band positions of PENBD in transmission spectra (ambient pressure) and multilayer spectra (UHV), and assignment to vibrational modes.

Assignment	Wavenumber [cm^{-1}]		
	DFT	Transmission IR	IRRAS
$\nu(C–H)_{as+s\ Phenyl}$	3125 + 3116	2982	2983
$\nu(C–H)_{as\ Ester}$	3055	2937	2940
$\nu(C–H)_{s\ Ester+NBD}$	2974	2870	2869
$\nu(C{=}O)_{as\ Ester}$	1683[a]	1693	1703
$\nu(C–C)_{as\ Phenyl}$ + $\delta(C–C)_{NBD}$	1592[a] + 1563[a]	1595 + 1558	1595 + 1558
$\nu(C–C)_{as\ Phenyl}$	1478[a]	1492	1493
$\delta(C–C)_{NBD}$	1276[a] + 1200[a] + 1131[a] + 1088 + 1059	1295 + 1236 + 1181 + 1100 + 1074	1296 + 1242 + 1191 + 1103 + 1076
$\nu(C–C–O)_{Ester}$	1029	1022	1035
$\delta(C–C)_{Phenyl}$ + $\delta(C–C)_{NBD}$	752 + 709 + 678	762 + 719 + 696	766 + 723 + 696

[a] Published in Ref. [34].

Table 2. IR band positions of PEQC in transmission spectra (ambient pressure) and multilayer spectra (UHV), and assignment to vibrational modes.

Assignment	Wavenumber [cm^{-1}]		
	DFT	Transmission IR	IRRAS
$\nu(C–H)_{as+s\ Phenyl}$	3125 + 3110	2987	2976
$\nu(C–H)_{as\ Ester}$	3055	2929 + 2945	2933
$\nu(C–H)_{s\ Ester}$	2973	2857	2862
$\nu(C{=}O)_{as\ Ester}$	1711[a]	1692	1716
$\nu(C–C)_{as\ Phenyl}$	1601[a]	1602	1604
$\nu(C–C)_{as\ Phenyl}$	1490[a]	1445	1446
$\nu(C–C)_{as\ Ester}$	1379[a] + 1361[a]	1409 + 1377	1408 + 1381
$\delta(C–C)_{QC}$	1282 + 1208[a] + 1153[a] + 1091 + 1025	1297 + 1236 + 1187 + 1122 + 1024	1304 + 1238 + 1113 + 1051 + 968
$\delta(C–C)_{Phenyl}$ + $\delta(C–C)_{QC}$	899 + 849 + 743	811 + 757 + 702	810 + 760 + 697

[a] Published in Ref. [34].

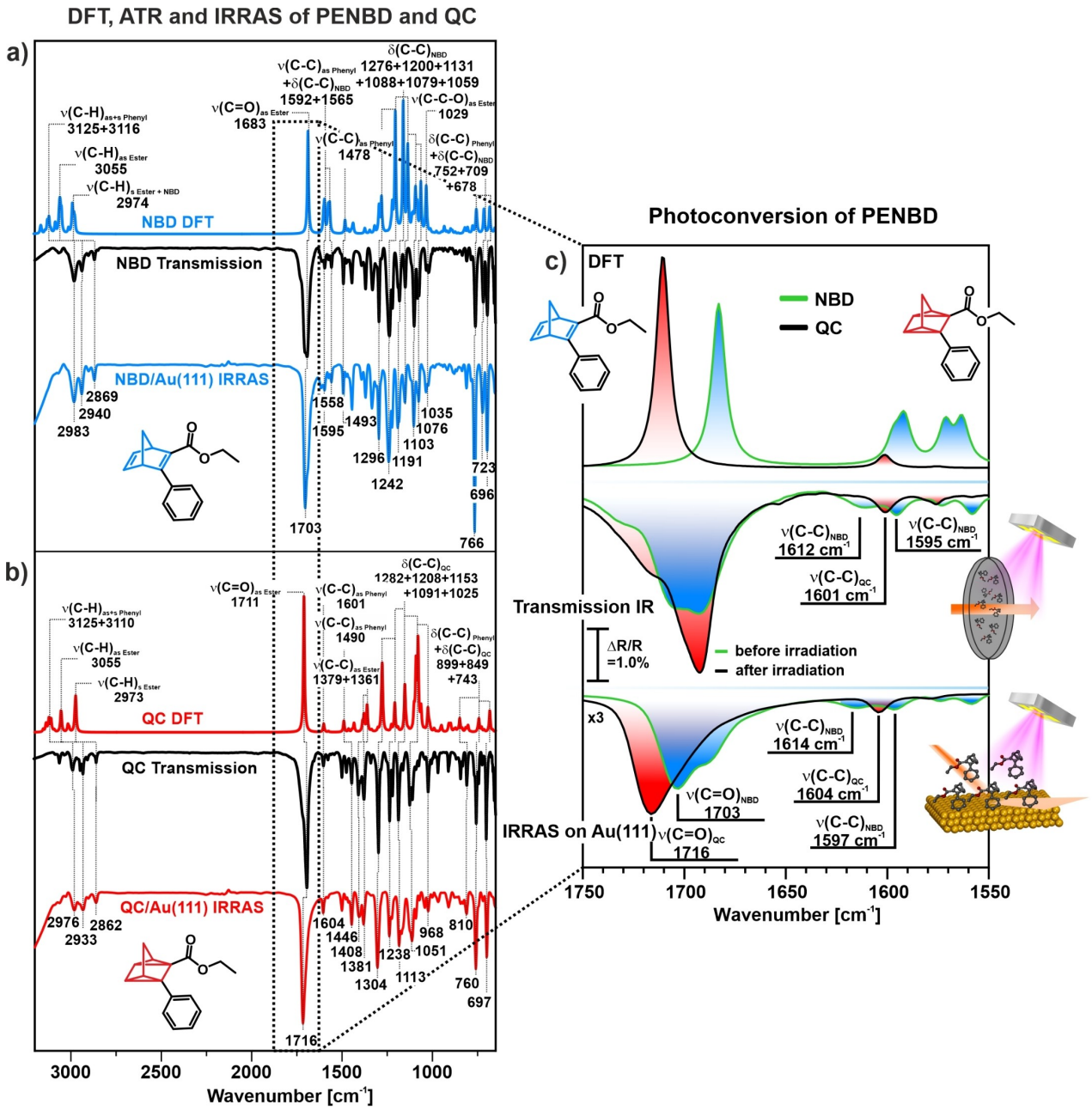

Figure 2. DFT calculated gas-phase IR, transmission IR in bulk solution, and multilayer IRRAS of a) PENBD and b) PEQC; c) Characteristic spectral region (1750 to 1550 cm^{-1}) before and after UV irradiation (128 scans (liquid phase), 256 s (UHV); see experimental) in identical order: DFT gas-phase spectra of PENBD (green spectrum with blue underlay) to PEQC (black spectrum with red underlay) as reference spectra (top); transmission IR spectra of PENBD/PEQC in KBr (middle) and IRRA multilayer spectra on Au(111) at 110 K (bottom). Significant bands are labelled. DFT and transmission IR spectra are adapted with permission from Ref. [34] under terms of the CC-BY 4.0 license. Copyright (2022), the Authors, published by Wiley-VCH.

observed a good agreement between the calculated IR spectra, the transmission spectra under ambient conditions, and the multilayer spectra in UHV. This demonstrated that PENBD can be deposited by PVD without decomposition. The complete disappearance of the bands at 1614 and 1596 cm^{-1}, specific for PENBD, as well as the appearance of the band at 1604 cm^{-1}, specific for PEQC, after irradiation in UHV indicated that PENBD can be photochemically converted to PEQC in a quantitative manner even under surface science conditions.

PEC-IRRAS in liquid phase

We studied the photochemical conversion and the catalytically triggered back-conversion of PENBD/PEQC on Au(111) in the liquid phase *in situ* by PEC-IRRAS (see Figure 3a). During the reaction, we applied a potential of $-0.7\ V_{fc}$ to the Au electrode. Note that we could tune the reaction rate by the applied potential as demonstrated in our previous work.[35] The corresponding spectra at open circuit potential (OCP) are provided in the Supporting Information (see Figure SI 1). We

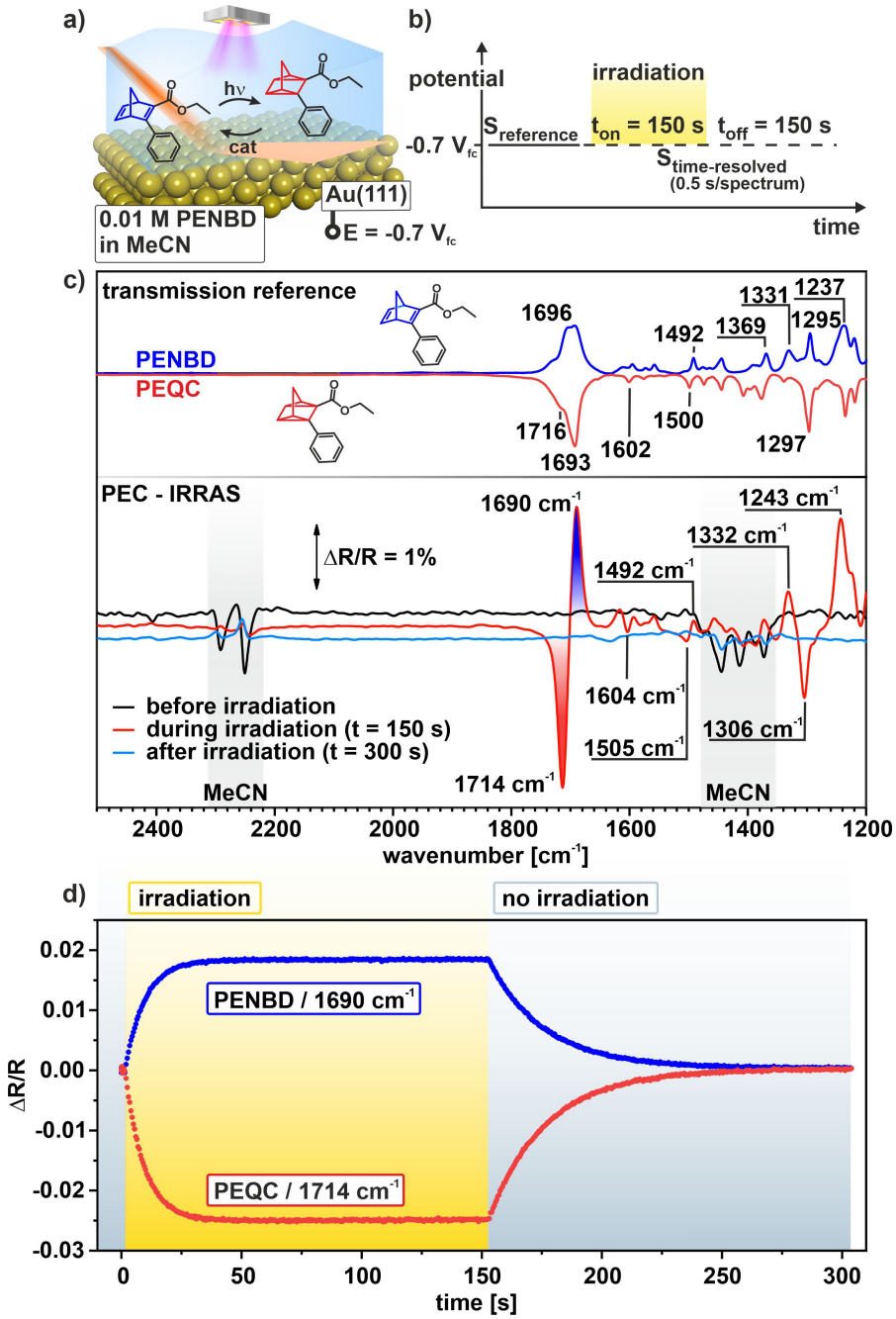

Figure 3. Photochemical conversion and catalytically triggered back-conversion of the PENBD/PEQC system in the liquid phase; a) Schematic representation of the energy storage and release; b) Experimental procedure; c) Transmission spectra of PENBD and PEQC and selected spectra before, during, and after irradiation measured during the *in situ* experiment; d) Peak intensity of the ν(CO) band of PENBD and PEQC during irradiation and catalytically triggered back-conversion; all spectra were acquired with 10 mM PENBD in 0.1 M Bu_4NClO_4 in MeCN at −0.7 V_{fc}.

measured PEC-IRRA spectra in thin-layer configuration using a spacer of 25 μm thickness. In this thin-layer configuration, the reactant exchange between the thin layer and the bulk solution is suppressed.[57] In previous work, we demonstrated that with this setup NBD diffusion from the thin layer to the bulk solution takes ~260 min. As a light source we used a UV-LED with λ_{max} = 310 nm (30 mW). A scheme of the experimental procedure is shown in Figure 3b. First, a reference spectrum and one additional spectrum were recorded before irradiation. Next, IR spectra (acquisition time = 0.5 s) were recorded during and after the irradiation (300 s per cycle). Figure 3c upper part shows the transmission reference spectra of PENBD (blue) and PEQC (red). For the most intense band around 1700 cm^{-1}, the ν(CO) stretching vibration, conversion led to a band shift which gave rise to a s-shaped band in the difference spectra. We used the ν(CO) band as a spectroscopic marker to follow the conversion and back-conversion. In the bottom part of Figure 3c, we show three selected PEC-IRRA spectra. One

before irradiation, one during irradiation, and one after the LED was switched off. Before irradiation, we did not observe any bands of PENBD or PEQC in the difference spectra, indicating stable conditions. Note that small bands at 1450 and 2250 cm^{-1} belong to the solvent acetonitrile[58] and indicated minimal changes of the layer thickness. During irradiation, we observed positive features for PENBD at 1690 cm^{-1} (ν(CO)), 1492 cm^{-1} ($\delta(CH)_{phenyl}$), 1332 cm^{-1} ($\delta(CH)_{phenyl}$), and 1243 cm^{-1} ($\delta(CH)_{NBD}$). For PEQC, we observed negative bands at 1714 cm^{-1} (ν(CO)), 1604 cm^{-1} ($\nu(CC)_{phenyl}$), 1505 cm^{-1} ($\delta(CH)_{phenyl}$), and 1306 cm^{-1} ($\nu(CC)_{QC,\ ester}$). Note that all spectra are difference spectra referred to the spectrum before irradiation. Therefore, positive bands (pointing upwards) indicate consumed species, while negative bands (pointing downwards) indicate formed species. The bands demonstrate the conversion of PENBD to PEQC upon irradiation. After irradiation, all bands vanished showing that all PEQC is back-converted to PENBD. In addition, we did not observe any other bands, which would indicate the formation of a side product. For a more detailed analysis, we will focus on the most intense bands, i.e., the ν(CO) bands. The intensity of these bands is plotted in Figure 3d. Upon irradiation, the intensity of both peaks increased very quickly and reached a plateau after ~50 s ($t_{1/2}$ = 7.5 s). After the LED is switched off, the intensity rapidly decreased and vanished completely after ~150 s ($t_{1/2}$ = 17 s). The increase in peak intensity during irradiation indicated photoconversion of PENBD to PEQC. As the Au(111) surface is present during irradiation, PEQC was continuously back-converted. After ~50 s of irradiation, the system reached steady state condition. After switching off the LED, all PEQC was back-converted to PENBD. In previous work, we determined the rate constant for the back-conversion of 2-cyano-3-(3,4-dimethoxyphenyl)-NBD/QC on Au(111) to be 5.8×10^{-6} $m{\cdot}s^{-1}$ at −0.7 V_{fc}.[35] As the half-life times of the conversion and back-conversion are very similar to the ones in the former study, we conclude that the reaction rate of the back-conversion on Au(111) is similar for both systems.

In the next step, we tested the cyclability of the system. We repeated the experiment described in Figure 3b for 100 times (Figure 4a). Note that we applied a potential of −0.7 V_{fc} during the experiment. In Figure 4b and **c**, we depict the ν(CO) region recorded during the first and the last cycles (cycle 1–3 and cycle 100–103) and the intensities of the ν(CO) bands for different cycles (spectra from 2500 to 1200 cm^{-1} are provided in Figure SI 2). Within the 100 storage cycles, PEQC was always back-converted completely to PENBD. We did not observe the formation of any side product. From this observation, we conclude that the system is fully reversible within the detection limits of our experiment. These results are in agreement with our previous work on the catalytic back-conversion of 2-cyano-3-(3,4-dimethoxyphenyl)-QC on Au(111).[35]

Finally, we inspected the stability of the reaction system. From our observation that the system is fully reversible, we conclude that the kinetics of the photochemical conversion are unaffected. Consequently, we can use the band intensity in the steady state to analyze the changes of the back-conversion rate qualitatively. We observed that the peak intensity is nearly constant over the 100 cycles and even decreased slightly with increasing cycle number. From this observation, we conclude that the catalytic activity remained stable within the 100 conversion cycles. Notably, the activity of the Au(111) surface was even increasing slightly with more frequent cycling. We attribute this favorable effect to reductive decomposition of impurities or poisoning species, which are present in the beginning after sample preparation (the exact nature cannot be determined on the basis of the present experiments). In summary, our results demonstrate very high catalytic activity and selectivity of Au(111) for energy release in the PENBD/PEQC system in the liquid phase.

Monolayer conversion with SRPES in UHV

In the next step, we address the catalytic energy release by surface science methods. We started with SRPES measurements of PEQC and PENBD at submonolayer coverages to obtain information on the activity of the compounds in direct contact with the gold surface and their reaction pathways upon heating. We followed the adsorption and thermal evolution of the photoswitches *in situ* in the C 1s and O 1s regions (see complete data sets in Figure SI 3 and SI 4). The catalyst surface was a gold film prepared by PVD and subsequent annealing[52] on a Pt(111) single crystal (see experimental section). This preparation led to a well-ordered surface structure[53] with a behavior in photoemission experiments identical to that of Au(111).[54]

Selected C 1s spectra are shown in Figure 5a. The red spectrum was acquired after exposure of the gold surface to PEQC at 110 K, yielding a total carbon coverage of 0.24 ML. In Figure 5b, we provide the corresponding quantitative analysis of the TP-SRPES experiment with PEQC, showing the carbon coverage as a function of temperature.

Interestingly, there were no pronounced differences in the spectral appearance when compared to PENBD (blue spectrum in Figure 5a) after adsorption of comparable amounts (0.32 ML) at 110 K, indicating the existence of equivalent surface species. The C 1s spectra of both PEQC and PENBD in Figure 5a featured a relatively broad signal with a main contribution at 284.3 eV and a distinct shoulder at 285.7 eV. In addition, smaller peaks at ~287.8 eV were found in both spectra. While the NBD/QC framework and phenyl moiety without heteroatoms are expected to contribute to the main signal at 284.3 eV, carbon atoms in vicinity to the oxygen atoms of the ester group were likely to add intensity at higher binding energies. Our observations suggest that the reaction of PEQC to PENBD already took place immediately upon adsorption. We attribute this spontaneous conversion at 110 K to the high catalytic activity of the gold surface leading to an instantaneous cycloreversion to PENBD. Therefore, no PEQC was observed spectroscopically even at low temperatures. Spectra of the O 1s region also confirmed the conversion (see Figure SI 5). The direct reconversion of PEQC under cryogenic temperatures is in agreement with previous experiments on

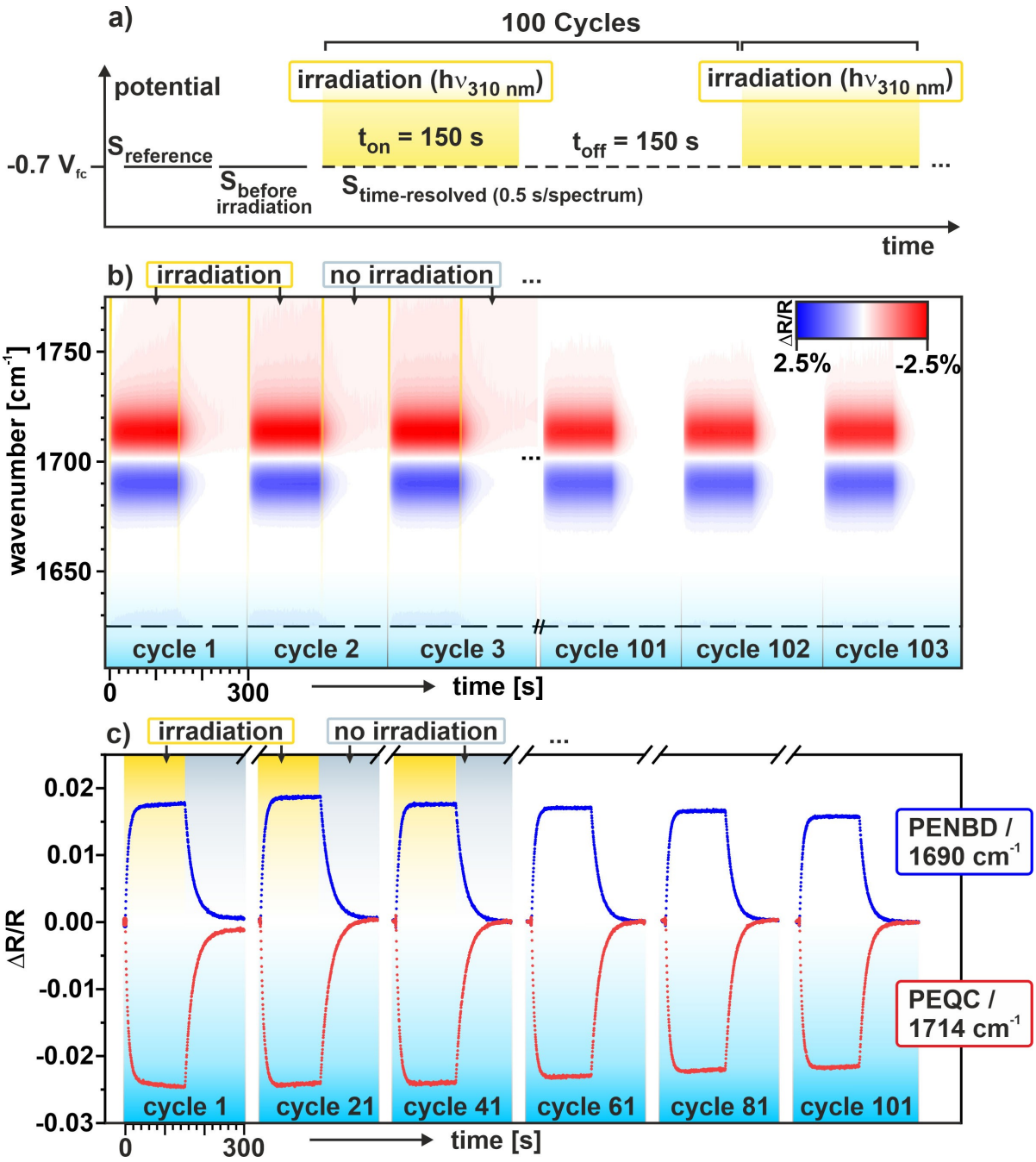

Figure 4. Stability of the PENBD-PEQC/Au(111) system probed over 100 storage and release cycles (between steady state and total back-conversion); a) Schematic presentation of the experimental procedure; b) Color plot of the ν(CO) region of the IR spectra recorded during cycle 1–3 and 101–103; c) Band intensity of ν(CO) bands of PENBD (1690 cm^{-1}) and PEQC (1714 cm^{-1}) during cycle 1, 21, 41, 61, 81, and 101.

Au(111), where the NBD/QC derivative was assembled on the Au(111) surface by means of a trioxatriangulene anchor platform.[38] We suggest that the reaction follows the same singlet-triplet mechanism as originally proposed by Herges, Magnussen, Tuczek, and co-workers for the catalytic back-conversion of azobenzene-based MOST photoswitches on Au(111).[29] The intersystem crossing between singlet and triplet states of the MOST molecules is mediated by the gold surface and represents a reaction pathway that minimizes the probability for uncontrolled side reactions. Figure SI 6 schematically depicts the energy landscape of the reaction system during the isomerization process.

In the following, we investigated the thermal evolution to obtain a more detailed view on the reaction behavior of PENBD. Starting at 135 K (see Figure SI 4 for details), a shift of the main signal at 284.3 eV occurred by about 150 meV towards higher binding energies. Simultaneously, the shoulders at the higher binding got considerably less intense and noticeably broader (light blue spectrum at 170 K in Figure 5a). This most striking change concerns the carbon atoms

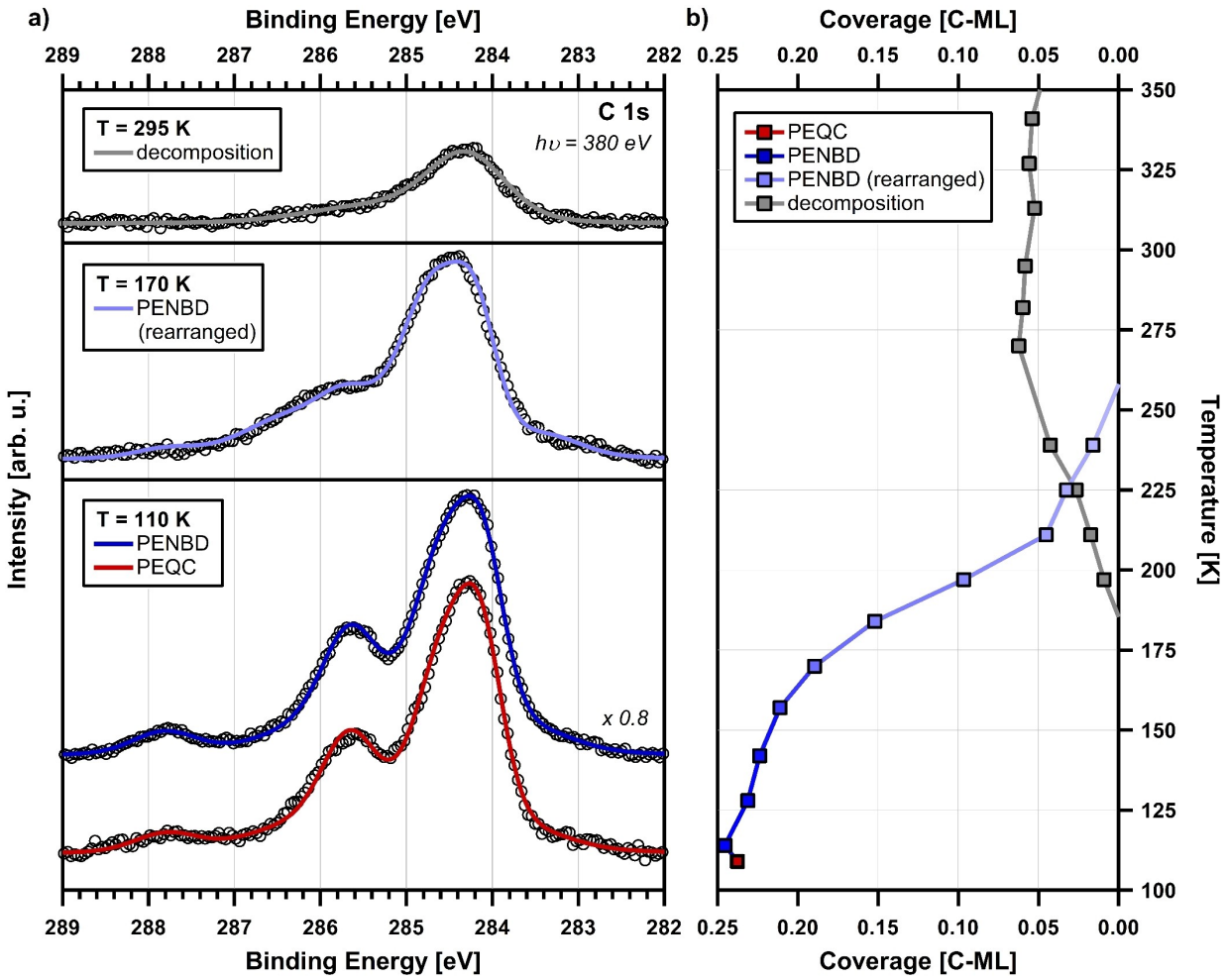

Figure 5. Selected SRPE spectra and quantitative analysis of the PEQC experiment; a) C 1s spectra at representative temperatures. There is no spectral distinction upon adsorption of PEQC and PENBD (rescaled) indicating an instantaneous cycloreversion reaction; rearrangement of PENBD occurs upon heating, and desorption of PENBD proceeds up to 250 K, with minor residues remaining on the surface (promoted by defects in gold film); b) Carbon coverage in monolayers upon thermal evolution.

influenced by the oxygen of the ester moiety, suggesting that the substituent can adopt different adsorption configurations. Since the spectral differences between 110 and 170 K were small, we propose that the molecules rearranged to a more stable adsorption geometry, as also observed for other NBD/QC systems.[37,42] While there was only a slight decline in carbon coverage below 150 K (less than 10%), a much more pronounced decrease was found up to 210 K (see Figure 5b). Beginning at 190 K, the line shape was described by an asymmetric peak at 284.3 eV (grey spectrum). This contribution is ascribed to carbonaceous fragments on the surface. These decomposition products were the only detected surface species above 250 K. The remaining coverage of ~0.05 ML, after the desorption of intact PENBD, was about 20% of the initial carbon amount. The obtained spectra at these temperatures match with literature values for carbide formation on polycrystalline gold.[59] This fragmentation was likely promoted by defects in the prepared gold films, as anticipated by theory for under-coordinated sites on gold.[60]

Our results demonstrate that the cycloreversion reaction on Au(111) took place at submonolayer coverages even at cryogenic temperatures of 110 K. Rearrangement of PENBD started at ~135 K, with the photoswitch adopting its most favorable adsorption geometry. Heating to >250 K, all PENBD has desorbed molecularly from the submonolayer, leaving minor residues on the surface due to decomposition at defects of the gold film.

Growth of mono and multilayer films of PENBD on Au(111)

The question remains, how the photoisomers behave at multilayer coverage. To address this question, we investigated the growth of PENBD films by IRRAS. We recorded time-resolved IRRA spectra during deposition of PENBD on clean Au(111) at 110 K in UHV (see Figure 6). At submonolayer coverage, the most prominent signal was the $\nu(C\text{–}C\text{–}O)_{Ester}$ vibration at 1052 cm^{-1} (Figure 6a and b). Note that only components of the dynamic dipole moment perpendicular to

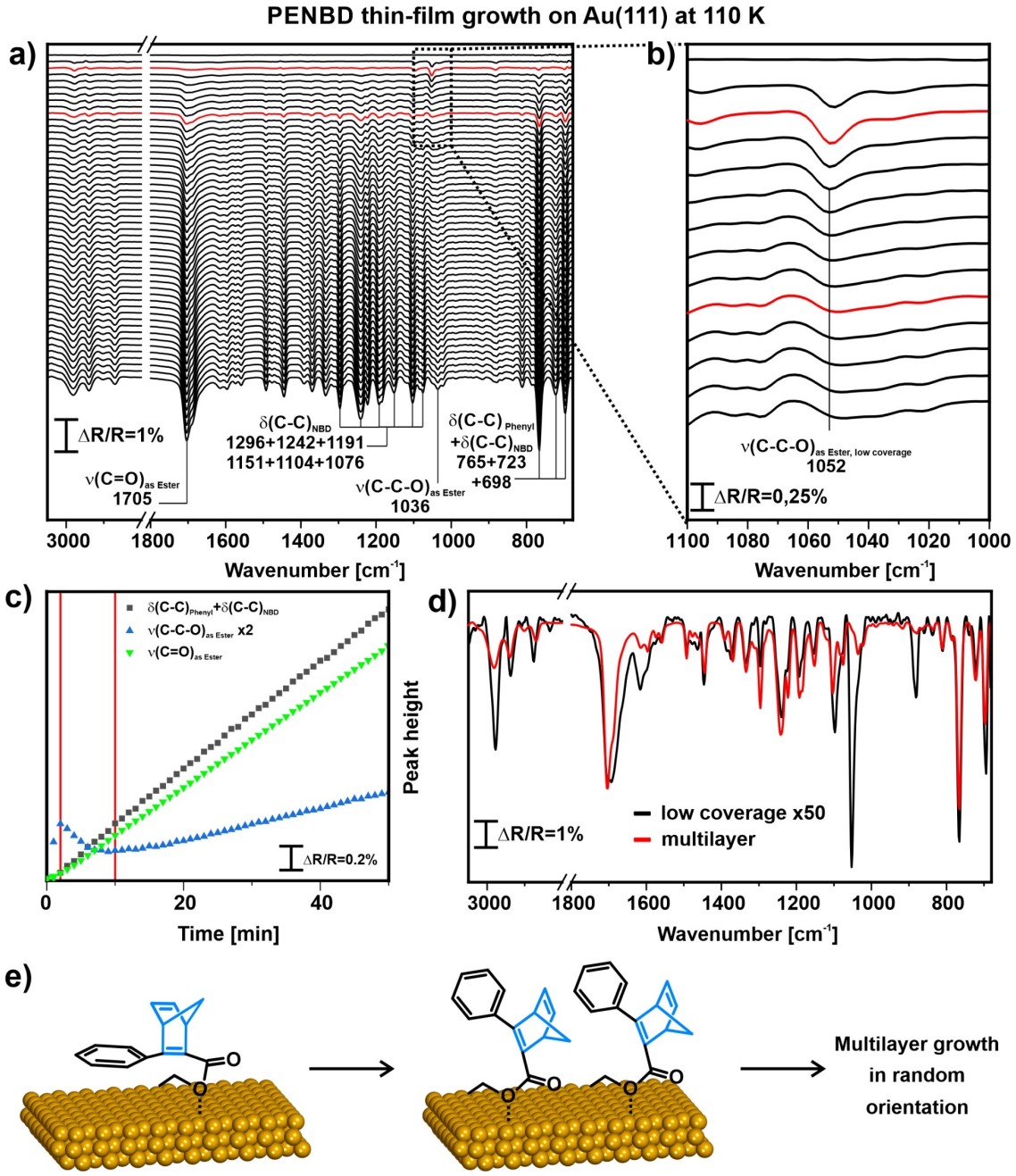

Figure 6. a) *In situ* IRRA spectra measured during PVD of PENBD on Au(111) at 110 K. For clarity, only the first 50 spectra are shown; b) Zoomed in portion of (a) at the ν(C–C–O)$_{as\ Ester}$ band at low coverage; c) Integrated band intensity of selected vibrational modes plotted as a function of deposition time. The integrated bands are δ(C–C)$_{Phenyl}$ + δ(C–C)$_{NBD}$ (739 to 798 cm^{-1}), ν(C–C–O)$_{as\ Ester}$ (997 to 1061 cm^{-1}), and ν(C=O)$_{as\ Ester}$ (1637 to 1784 cm^{-1}); d) Comparison of the PENBD monolayer (scaled by 50 times) and the multilayer; e) Reorientation of PENBD in the (sub)monolayer.

the surface plane give rise to absorption due to the metal surface selection rule (MSSR).[61–63] Therefore, we conclude that the ester group of this PENBD molecule adsorbed in an upright-standing binding motif. With increasing coverage, the ν(C–C–O)$_{Ester}$ signal decreased in intensity and redshifted from 1052 to 1036 cm^{-1} in the multilayer. This indicated change of orientation on the Au(111) surface. In parallel, new bands appeared close to the positions of the multilayer (see Table 1). In addition, we observed changes in the relative band intensities (see Figures 6c and d showing scaled spectra of the monolayer at low coverage and of the multilayer). These changes in intensity indicated a reorientation of the adsorbed PENBD molecules (see Figure 6e). After the first 10 minutes, all bands grew linearly suggesting a random orientation of the adsorbing molecules in the multilayer.

Thermal stability and back-conversion of PEQC in UHV

Finally, we converted the multilayer of PENBD photochemically and studied its back-conversion upon heating by TP-IRRAS (from 110 to 700 K). In the color plot in Figure 7a, we show the multilayer spectra with a background spectrum measured after desorption at 700 K. These spectra represent all species present on the surface (denoted as 'absolute spectra'). In the color plot in Figure 7b, we show all spectra always using the previously recorded spectrum as background. These spectra represent the differential changes while heating ('differential' spectra). Positive bands indicate a loss of band intensity, while negative bands indicate a gain in band intensity.

From 110 to 150 K, we observed bands in the absolute spectra at the positions of the multilayer spectrum of PEQC. In this temperature range, the spectra did not change (no signals

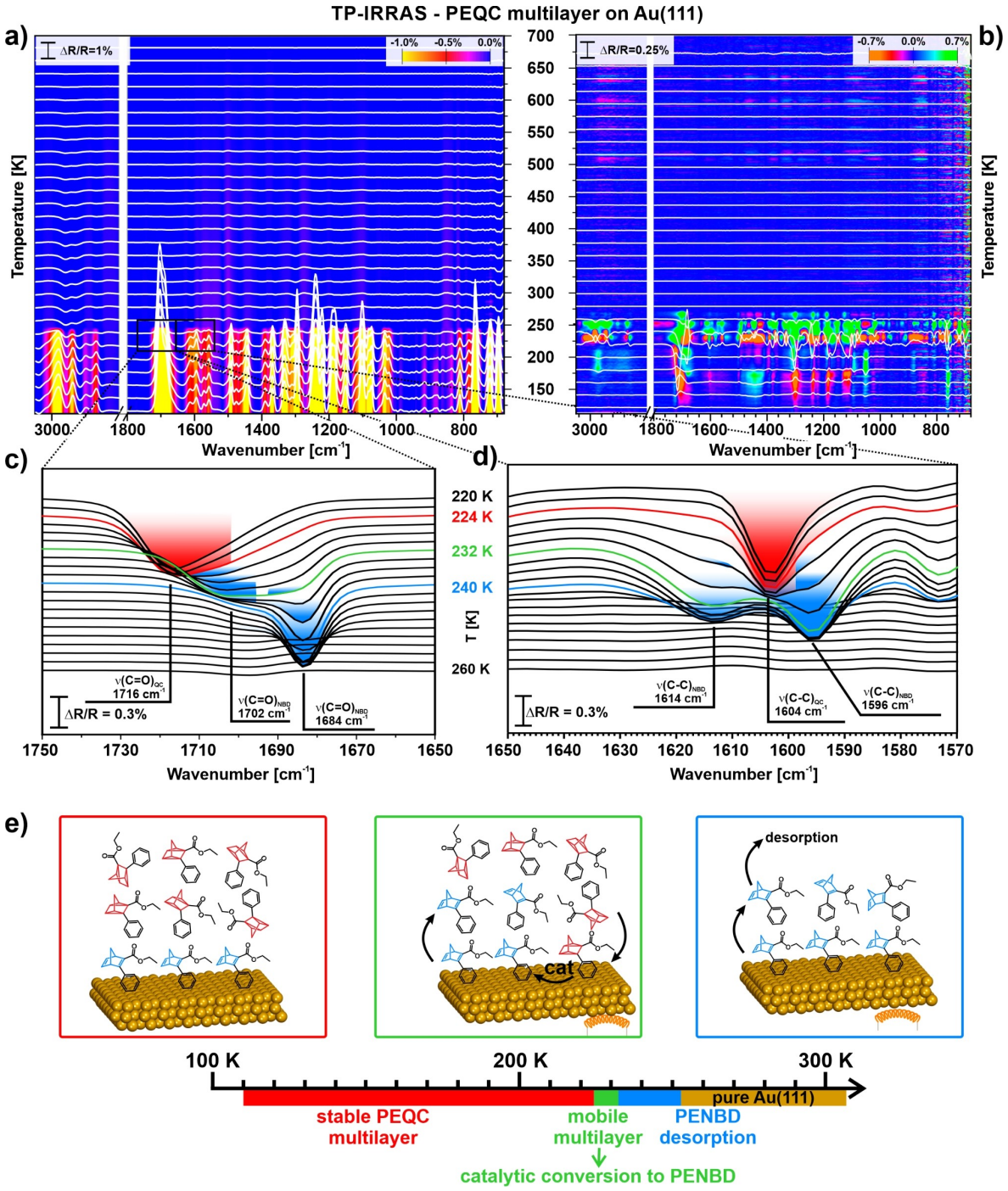

Figure 7. a) TP-IRRAS of a PEQC multilayer from 110 to 700 K plotted as absolute spectra in a color plot (see experimental); b) TP-IRRAS of a PEQC multilayer from 110 to 700 K plotted as relative spectra in a color plot (see experimental); c) Enlarged detail of the absolute spectra in the $\nu(C{=}O)_{as}$ region (1750 to 1650 cm^{-1}) from 220 to 260 K; d) Enlarged detail of the absolute spectra in the $\nu(C{-}C)_{QC/NBD}$ region (1650 to 1570 cm^{-1}); e) Schematic model of the catalytic back-conversion on the gold surface.

in the differential spectra). From 150 to 224 K, we observed changes in the band ratios (see differential spectra). From 224 to 232 K, the band at 1716 cm^{-1} vanished, and two new bands appeared at 1702 cm^{-1} and 1684 cm^{-1}. The latter band became the dominant band at temperatures > 232 K (see inset in Figure 7c). In the region around 1600 cm^{-1}, we observed that the band at 1604 cm^{-1} vanished between 224 and 232 K, while two new bands appeared at 1614 and 1596 cm^{-1} (inset 7 d). Above 250 K, these bands disappeared.

The changes of band ratios between 150 and 224 K indicated a change of film morphology. The spectral changes in the temperature range between 224 and 232 K suggested that PEQC converts back to PENBD in a narrow temperature range. We propose that in this temperature region, the molecules in the film became mobile, so all PEQC species got in direct contact with the gold surface and were back-converted to PENBD. The loss of signal intensity above 232 K was attributed to the desorption of the multilayer. Note that the band at 1684 cm^{-1} corresponds to the ν(C=O) mode of a molecule, which is in direct contact to the gold surface. Above 240 K, the PENBD monolayer started to desorb. We attribute the lower desorption temperature in the SRPES experiments to the different starting conditions (submonolayer coverage vs. multilayer coverage). In Figure 7e, we schematically depict the behavior at different temperatures. Up to 224 K, the multilayer of PEQC was stable and only some rearrangements in the frozen film took place. Between 224 and 232 K, the multilayer film became so mobile that all PEQC molecules came in contact with the Au(111) surface and were directly back-converted to PENBD. Above 232 and 240 K, the multilayer and monolayer desorbed, respectively.

Conclusions

In summary, we studied the mechanism and reversibility of energy release from a norbornadiene-based molecular solar thermal (MOST) system combining liquid-phase and surface science experiments. Specifically, we studied the promising MOST system phenylethylesternorbornadiene/quadricyclane (PENBD/PEQC) on catalytically active Au(111) by photoelectrochemical infrared reflection absorption spectroscopy (PEC-IRRAS) in the liquid phase (reaction kinetics and reversibility), synchrotron radiation photoelectron spectroscopy (SRPES) in ultra-high vacuum (UHV) (mechanism, monolayer conversion), and UHV-based IRRAS (mechanism, bulk conversion).

Our main conclusions are summarized as follows:

(1) Activity: The Au(111) surface triggers the energy release of PEQC in the liquid phase with very high activity. The back-conversion is fully completed within 150 s. The release rate of the heterogeneously catalyzed back-conversion of PEQC can be tuned by applying an external potential.
(2) Reaction mechanism: In UHV, (sub)monolayers of PEQC, which are in contact with the Au(111) surface, convert directly back to PENBD, even at cryogenic temperatures (110 K). We attribute the back-conversion to the same singlet-triplet mechanism previously reported for other photoswitches.[29,38] The reaction is induced by direct electronic coupling between the Au(111) surface and PEQC. In the multilayer, where the photoswitch is electronically decoupled from the Au(111) surface, PEQC is stable up to temperatures of 220 K. Above this temperature, the frozen film becomes mobile, all PEQC reaches the Au(111) surface, and is back-converted to PENBD.
(3) Desorption: In UHV, we observe desorption of the multilayer at temperatures above 232 K (IRRAS). At submonolayer coverage, PENBD first rearranges at temperatures of ~135 K into the energetically most favorable adsorption geometry. At elevated temperatures of > 250 K, all PENBD has desorbed from the submonolayer, leaving minor residues on the surface promoted by defects in the gold film (SRPES).
(4) Reversibility: In the liquid phase, the back-conversion on Au(111) is highly selective and within numerous conversion cycles we do not observe any decomposition. Within 100 cycles, no deactivation occurs and the activity of the Au(111) surface even increases slightly, possibly due to removal of contaminants.

Our multi-method study demonstrates the outstanding catalytic properties of gold as a heterogeneous catalyst for the energy release from NBD-based MOST systems and provides additional mechanistic information required for further knowledge-driven catalyst development.

Supporting Information

The authors have cited additional references within the Supporting Information (Ref. [64–66]).

Acknowledgements

The authors acknowledge financial support by the Deutsche Forschungsgemeinschaft (DFG) within the Research Unit FOR 5499 "Molecular Solar Energy Management – Chemistry of MOST Systems" (project 496207555) and project 392607742. The authors acknowledge additional support by the DFG (Collaborative Research Centre SFB 1452 – Catalysis at Liquid Interfaces, Research Unit FOR 1878 "Functional Molecular Structures on Complex Oxide Surfaces" (project 214951840) and further projects (431733372, 453560721, 322419553)), the German Federal ministry of Education and Research (BMBF, Project Combined Infrared and X-Ray Analytics of Energy Materials, CIXenergy 05 K19WE1), the Bavarian ministry of Economic Affairs, Regional Development and Energy, and the Cluster of Excellence "Engineering of Advanced Materials". We thank Helmholtz-Zentrum Berlin for the allocation of synchrotron radiation beamtime and the BESSY II staff for support during beamtime. We also thank Yannick Wingerter from the group of Prof. Dr. Hirsch for measuring the UV/Vis spectra of PENBD and PEQC. Open Access funding enabled and organized by Projekt DEAL.

Conflict of Interests

The authors declare no conflict of interest.

Data Availability Statement

The data that support the findings of this study are presented in the Manuscript and the Supplementary Information. Source data are provided at Zenodo: DOI https://zenodo.org/doi/10.5281/zenodo.10022604.

Keywords: norbornadiene · photoswitches · quadricyclane · solar energy storage · surface chemistry

[1] T. J. Kucharski, Y. Tian, S. Akbulatov, R. Boulatov, *Energy Environ. Sci.* **2011**, *4*, 4449–4472.
[2] A. Lennartson, K. Moth-Poulsen, in *Molecular Devices for Solar Energy Conversion and Storage*, Springer, Singapore, **2018**, pp. 327–352.
[3] Z. Wang, A. Roffey, R. Losantos, A. Lennartson, M. Jevric, A. U. Petersen, M. Quant, A. Dreos, X. Wen, D. Sampedro, K. Börjesson, K. Moth-Poulsen, *Energy Environ. Sci.* **2019**, *12*, 187–193.
[4] Z. Wang, P. Erhart, T. Li, Z.-Y. Zhang, D. Sampedro, Z. Hu, H. A. Wegner, O. Brummel, J. Libuda, M. B. Nielsen, K. Moth-Poulsen, *Joule* **2021**, *5*, 3116–3136.
[5] T. J. Kucharski, N. Ferralis, A. M. Kolpak, J. O. Zheng, D. G. Nocera, J. C. Grossman, *Nat. Chem.* **2014**, *6*, 441–447.
[6] A. Goulet-Hanssens, M. Utecht, D. Mutruc, E. Titov, J. Schwarz, L. Grubert, D. Bléger, P. Saalfrank, S. Hecht, *J. Am. Chem. Soc.* **2017**, *139*, 335–341.
[7] Z. F. Liu, K. Hashimoto, A. Fujishima, *Nature* **1990**, *347*, 658–660.
[8] A. H. Heindl, H. A. Wegner, *Chem. A Eur. J.* **2020**, *26*, 13730–13737.
[9] J. H. Griwatz, A. Kunz, H. A. Wegner, *Beilstein J. Org. Chem.* **2022**, *18*, 781–787.
[10] E. Franz, A. Kunz, N. Oberhof, A. H. Heindl, M. Bertram, L. Fusek, N. Taccardi, P. Wasserscheid, A. Dreuw, H. A. Wegner, O. Brummel, J. Libuda, *ChemSusChem* **2022**, *15*, e202200958.
[11] E. Franz, J. Jung, A. Kunz, H. A. Wegner, D. Mollenhauer, O. Brummel, J. Libuda, *J. Phys. Chem. Lett.* **2023**, *14*, 1470–1477.
[12] S. L. Broman, M. B. Nielsen, *Phys. Chem. Chem. Phys.* **2014**, *16*, 21172–21182.
[13] C. Schøttler, S. K. Vegge, M. Cacciarini, M. B. Nielsen, *ChemPhotoChem* **2022**, *6*, e202200037.
[14] M. D. Kilde, M. Mansø, N. Ree, A. U. Petersen, K. Moth-Poulsen, K. V. Mikkelsen, M. B. Nielsen, *Org. Biomol. Chem.* **2019**, *17*, 7735–7746.
[15] K. Edel, X. Yang, J. S. A. Ishibashi, A. N. Lamm, C. Maichle-Mössmer, Z. X. Giustra, S. Y. Liu, H. F. Bettinger, *Angew. Chem. Int. Ed.* **2018**, *57*, 5296–5300.
[16] A. D. Dubonosov, V. A. Bren, V. A. Chernoivanov, *Russ. Chem. Rev.* **2002**, *71*, 917–927.
[17] V. A. Bren', A. D. Dubonosov, V. I. Minkin, V. A. Chernoivanov, *Russ. Chem. Rev.* **1991**, *60*, 451–469.
[18] C. Schuschke, C. Hohner, M. Jevric, A. Ugleholdt Petersen, Z. Wang, M. Schwarz, M. Kettner, F. Waidhas, L. Fromm, C. J. Sumby, A. Görling, O. Brummel, K. Moth-Poulsen, J. Libuda, *Nat. Commun.* **2019**, *10*, 1–10.
[19] Z. Wang, H. Hölzel, K. Moth-Poulsen, *Chem. Soc. Rev.* **2022**, *51*, 7313–7326.
[20] Z. Wang, Z. Wu, Z. Hu, J. Orrego-Hernández, E. Mu, Z. Y. Zhang, M. Jevric, Y. Liu, X. Fu, F. Wang, T. Li, K. Moth-Poulsen, *Cell Reports Phys. Sci.* **2022**, *3*, 100789.
[21] "Solar radiation and photosynethically active radiation," can be found under http://www.fondriest.com/ environmental-measurements/parameters/ weather/photosynthetically-active-radiation, **2014**. (accessed on 2023–03-09).
[22] M. Jevric, A. U. Petersen, M. Mansø, S. Kumar Singh, Z. Wang, A. Dreos, C. Sumby, M. B. Nielsen, K. Börjesson, P. Erhart, K. Moth-Poulsen, *Chem. A Eur. J.* **2018**, *24*, 12767–12772.
[23] P. Lorenz, T. Luchs, A. Hirsch, *Chem. A Eur. J.* **2021**, *27*, 4993–5002.
[24] M. Quant, A. Lennartson, A. Dreos, M. Kuisma, P. Erhart, K. Börjesson, K. Moth-Poulsen, *Chem. A Eur. J.* **2016**, *22*, 13265–13274.
[25] J. Orrego-Hernández, A. Dreos, K. Moth-Poulsen, *Acc. Chem. Res.* **2020**, *53*, 1478–1487.
[26] Ken-ichi Hirao, A. Yamashita, O. Yonemitsu, *Tetrahedron Lett.* **1988**, *29*, 4109–4112.
[27] D. J. Fife, K. W. Morse, W. M. Moore, *J. Am. Chem. Soc.* **1983**, *105*, 7404–7407.
[28] U. Jung, C. Schütt, O. Filinova, J. Kubitschke, R. Herges, O. Magnussen, *J. Phys. Chem. C* **2012**, *116*, 25943–25948.
[29] A. Schlimm, R. Löw, T. Rusch, F. Röhricht, T. Strunskus, T. Tellkamp, F. Sönnichsen, U. Manthe, O. Magnussen, F. Tuczek, R. Herges, *Angew. Chem. Int. Ed.* **2019**, *58*, 6574–6578.
[30] J. L. Greenfield, M. A. Gerkman, R. S. L. Gibson, G. G. D. Han, M. J. Fuchter, *J. Am. Chem. Soc.* **2021**, *143*, 15250–15257.
[31] F. Waidhas, M. Jevric, L. Fromm, M. Bertram, A. Görling, K. Moth-Poulsen, O. Brummel, J. Libuda, *Nano Energy* **2019**, *63*, 103872.
[32] F. Waidhas, M. Jevric, M. Bosch, T. Yang, E. Franz, Z. Liu, J. Bachmann, K. Moth-Poulsen, O. Brummel, J. Libuda, *J. Mater. Chem. A* **2020**, *8*, 15658–15664.
[33] O. Brummel, D. Besold, T. Döpper, Y. Wu, S. Bochmann, F. Lazzari, F. Waidhas, U. Bauer, P. Bachmann, C. Papp, H.-P. Steinrück, A. Görling, J. Libuda, J. Bachmann, *ChemSusChem* **2016**, *9*, 1424–1432.
[34] E. Franz, D. Krappmann, L. Fromm, T. Luchs, A. Görling, A. Hirsch, O. Brummel, J. Libuda, *ChemSusChem* **2022**, *15*, e202201483.
[35] E. Franz, C. Stumm, F. Waidhas, M. Bertram, M. Jevric, J. Orrego-Hernández, H. Hölzel, K. Moth-Poulsen, O. Brummel, J. Libuda, *ACS Catal.* **2022**, *12*, 13418–13425.
[36] T. Luchs, P. Lorenz, A. Hirsch, *ChemPhotoChem* **2020**, *4*, 52–58.
[37] F. Hemauer, V. Schwaab, E. M. Freiberger, N. J. Waleska, A. Leng, C. Weiß, J. Steinhauer, F. Düll, P. Bachmann, A. Hirsch, H.-P. Steinrück, C. Papp, *Chem. A Eur. J.* **2023**, *29*, e202203759.
[38] R. Eschenbacher, T. Xu, E. Franz, R. Löw, T. Moje, L. Fromm, A. Görling, O. Brummel, R. Herges, J. Libuda, *Nano Energy* **2022**, *95*, 107007.
[39] G. Ertl, *Angew. Chem. Int. Ed.* **2008**, *47*, 3524–3535.
[40] U. Bauer, L. Fromm, C. Weiß, P. Bachmann, F. Späth, F. Düll, J. Steinhauer, W. Hieringer, A. Görling, A. Hirsch, H.-P. Steinrück, C. Papp, *J. Phys. Chem. C* **2019**, *123*, 7654–7664.
[41] U. Bauer, L. Fromm, C. Weiß, F. Späth, P. Bachmann, F. Düll, J. Steinhauer, S. Matysik, A. Pominov, A. Görling, A. Hirsch, H.-P. Steinrück, C. Papp, *J. Chem. Phys.* **2019**, *150*, 1847061–18470613.
[42] F. Hemauer, U. Bauer, L. Fromm, C. Weiß, A. Leng, P. Bachmann, F. Düll, J. Steinhauer, V. Schwaab, R. Grzonka, A. Hirsch, A. Görling, H.-P. Steinrück, C. Papp, *ChemPhysChem* **2022**, *23*, e202200199.
[43] U. Bauer, S. Mohr, T. Döpper, P. Bachmann, F. Späth, F. Düll, M. Schwarz, O. Brummel, L. Fromm, U. Pinkert, A. Görling, A. Hirsch, J. Bachmann, H.-P. Steinrück, J. Libuda, C. Papp, *Chem. A Eur. J.* **2017**, *23*, 1613–1622.
[44] O. Brummel, F. Waidhas, U. Bauer, Y. Wu, S. Bochmann, H.-P. Steinrück, C. Papp, J. Bachmann, J. Libuda, *J. Phys. Chem. Lett.* **2017**, *8*, 2819–2825.
[45] L. A. Kibler, *Int. Soc. Electrochem.* **2003**, 1–56.
[46] T. Xu, M. Schwarz, K. Werner, S. Mohr, M. Amende, J. Libuda, *Phys. Chem. Chem. Phys.* **2016**, *18*, 10419–10427.
[47] M. Schwarz, C. Schuschke, T. N. Silva, S. Mohr, F. Waidhas, O. Brummel, J. Libuda, *Rev. Sci. Instrum.* **2019**, *90*, 1–10.
[48] Helmholtz-Zentrum Berlin für Materialien und Energie, *JLSRF* **2016**, 2, A72.
[49] R. Denecke, M. Kinne, C. M. Whelan, H.-P. Steinrück, *Surf. Rev. Lett.* **2002**, *9*, 797–801.
[50] S. Doniach, M. Sunjic, *J. Phys. C Solid State Phys.* **1970**, *3*, 285–291.
[51] M. Kinne, T. Fuhrmann, C. M. Whelan, J. F. Zhu, J. Pantförder, M. Probst, G. Held, R. Denecke, H.-P. Steinrück, *J. Chem. Phys.* **2002**, *117*, 10852–10859.
[52] C. C. Leon, J. G. Lee, S. T. Ceyer, *J. Phys. Chem. C* **2014**, *118*, 29043–29057.
[53] J. W. A. Sachtler, G. A. Somorjai, *J. Catal.* **1983**, *81*, 77–94.
[54] B. Vogt, B. Schmiedeskamp, U. Heinzmann, *Zeitschrift für Phys. B Condens. Matter* **1990**, *80*, 359–364.
[55] A. Baraldi, G. Comelli, S. Lizzit, D. Cocco, G. Paolucci, R. Rosei, *Surf. Sci.* **1996**, *367*, L62–L67.
[56] C. Papp, H.-P. Steinrück, *Surf. Sci. Rep.* **2013**, *68*, 446–487.
[57] T. Iwasita, F. C. Nart, *Prog. Surf. Sci.* **1997**, *55*, 271–340.
[58] E. L. Pace, L. J. Noe, *J. Chem. Phys.* **1968**, *49*, 5317–5325.
[59] J. Luthin, C. Linsmeier, *Surf. Sci.* **2000**, *454*, 78–82.
[60] J. A. Herron, J. Scaranto, P. Ferrin, S. Li, M. Mavrikakis, *ACS Catal.* **2014**, *4*, 4434–4445.

[61] F. M. Hoffmann, *Surf. Sci. Rep.* **1983**, *3*, 107–192.
[62] H. A. Pearce, N. Sheppard, *Surf. Sci.* **1976**, *59*, 205–217.
[63] R. G. Greenler, D. R. Snider, D. Witt, R. S. Sorbello, *Surf. Sci.* **1982**, *118*, 415–428.
[64] M. A. Van Spronsen, K. J. Weststrate, A. Den Dunnen, M. E. Van Reijzen, C. Hahn, L. B. F. Juurlink, *J. Phys. Chem. C* **2016**, *120*, 8693–8703.
[65] B. D. Kay, K. R. Lykke, J. R. Creighton, S. J. Ward, *J. Chem. Phys.* **1989**, *91*, 5120–5121.
[66] R. G. Quiller, T. A. Baker, X. Deng, M. E. Colling, B. K. Min, C. M. Friend, *J. Chem. Phys.* **2008**, *129*, 0647021–0647029.

Manuscript received: October 20, 2023
Revised manuscript received: October 25, 2023
Accepted manuscript online: November 2, 2023
Version of record online: November 21, 2023